International Journal for Multidisciplinary Research (IJFMR)
E-ISSN: 2582-2160 ● Website: www.ijfmr.com ● Email: editor@ijfmr.com

Photocatalytic,Antimicrobial and Antifungal Activities of Cerium Oxide Doped with Manganese Dioxide Nanoparticles Using Karanja Leaves Extract

Thiruppathy J[1], Selvarani S[2], Abirami R[3]

[1]Assistant Professor, Department of Chemistry, Thiagarajar college, Madurai, Tamilnadu-625009, India.
[2]Associate Professor, Department of Zoology, Thiagarajar college, Madurai, Tamilnadu-625009, India
[3]Research Scholar, Thiagarajar college, Madurai, Tamilnadu-625009, India.

Abstract

In the present study, Cerium oxide doped with manganese dioxide nanoparticles were prepared using Karanja (Pongamia pinnata) leaves extract.The plant belongs to the Fabaceae family with common name karanja tree. The plant well distributed in Asia and Australia, used for treatment of skin diseases.This nanoparticles are utilised in photocatalytic dye degradation, anti-bacterial and anti-fungal activities. The synthesised nanoparticles were characterised and their activities are supported by powder X-ray diffractometer(PXRD),Energy-dispersiveX-ray spectroscopy(EDAX), Fourier transform Infra-red spectroscopy(FTIR), Scanning electron microscopy(SEM) and UV-Vis spectroscopy. The results showed that Cerium oxide doped with manganese dioxide nanoparticles using karanja leaves extract have zone of inhibition against Aspergillus niger and Aspergillus fumigatus in anti-fungal activity. It was also investigated that the extract have zone of inhibition against Staphylococcus aureus and E-coli in anti-microbial activity.

Keywords: 1.Cerium oxide, 2. Karanja, 3. MnO_2, 4. Photocatalytic, Anti-fungal and Microbial activity

1. Introduction

In recent development of science and technology, water pollution makes significant problem in the world. To degrade the organic pollutants in water using photo catalytic activity and also by mixing with natural leaves extract. Another way to degrade water pollutants are semiconductor photo catalyst [1,2] In which cerium oxide nanoparticles have been used as photocatalyst in many fields. [3], optical film material [4], auto-motive exhaust catalyst [5], ultraviolet shielding material [6], gas sensors, optoelectronics and microelectronics [7]. The band gap of 3.2 eV makes CeO_2 an efficient absorbent in UV region and a potential photocatalyst. In fact, nanostructured CeO_2 has emerged as the substitute for the conventional TiO_2 among the researchers for photocatalytic study [8].

In this study investigate a method to reduce the band gap of cerium oxide nanoparticles by doping it with MnO_2 ions and to find out anti-fungal, anti-microbial acivity mixed with Karanja extract. From previous Literature survey, the usage of photocatalytic activity of CeO_2 nanoparticles in degradation of methylene

blue [9], in degradation of an aqueous suspension
Keywords: Manganese-doped cerium oxide nanoparticles, Anthraquinone dye, Remazol brilliant blue R, Photodegradation.Asian Journal of Chemistry; Vol. 30, No. 11 (2018), 2544-255 have been widely explored for their photocatalytic activity towards environmental remediation in general and waste water treatment in particularly like acridine orange under UV light [10], congo red [11], rhodamine-B dye using visible light [12]. Due large band gap of 3.2 eV CeO_2allows only 3-5% of solar energy consists of UV-radiation [13].
The surface defect method is the one which traps the electrons and prevents recombination of electron and holes. In addition,it adsorbs dye molecules for degradation and increase photocatalytic activity. [14]. The number of transition metal ions like Fe [15], Au [16], Pd- [17], Mn [18], doped with CeO_2 nanoparticles.The doping of Mn ion with CeO_2 nanoparticles causes decrease in band gap and lowering energy of empty d-orbitals in Mn than 4f orbitals of Ce [19]. The 4f electronic configuration can enhance transfer of an electron from the adsorbed dye to oxygen species, thus increases the photocatalytic activity [20]. In the present study shows that the effect of Mn-doped CeO_2 nanoparticles synthesized by a facile aqueous coprecipitation method. The photocatalytic activity of pristine and Mn-doped CeO_2 nanoparticles have been investigated towards the degradation of anthraquinone dye remazol brilliant blue R under visible and UV irradiation. Remazol brilliant blue R is a reactive dye that contains alkyl sulphonate anchor group. Its non-biodegradability and recalcitrant nature harms aquatic life [21].
In this study, karanja extract is used to synthesize CeO_2doped with MnO_2nanoparticles. The plant used in this study belongs to the Fabaceae Family with common name karanja tree or malapuri plant. [22]. The synthesis of nanoparticles using the extracts of Cynodon dactylon, Cyprus rotundus grass [23], Verbascum thapsus [24], Brassica oleracea var. italic [25] and Cordia sebestena flower [26] are reported. Like CeO_2doped with MnO_2nanoparticles also have unique properties like chemical stability, catalytic and antimicrobial activity. The antimicrobial activities of CuO-Ag NPs prepared using Acalypha indica [27], Phyllanthus amarus [28], Terminalia arjuna [29], Calotropis gigantean [30], Malva sylvestris [31], Cassia alata and Carica papaya [32] have also been reported. All parts of Karanja tree are used for medicinal purposes. The phytoconstituents of this plant belongs to flavonoids and fixed oils. This medicinal plant is widely available in Western Ghats and tidal forests of India. The probable mechanisms for the photocatalytic dye degradation, anti-microbial and anti-fungal activities of the synthesized nanoparticles are discussed.

2. Experimental

2.1 Green synthesis of Cerioum Oxide doped with MnO_2 nanoparticles with karanja leaves extract

25 gms of fresh leaves of *karanja* cut into small pieces were taken and washed with distilled water then it is dried for few days, made into powder by using mortar. From this 10 gms of powder is taken in beaker add 100 ml of distilled water heated to 80° c for two hours. It is then filtered using whatman filter paper. 0.01M (5g) of Ceric Ammonium Nitrate is mixed with 17.5ml of water and 0.05M (5g) of Ammonium Carbonate is mixed with 17.5ml of water in a separate beaker and then mix it then add a 0.002M (0.5g)of Glucose is added and 0.02M (2g) of Manganese Dioxide is added in the mixture, it is kept in the magnetic stirrer for about 5hours and then it is kept in an oven for about 90 mins at 60°C

Graphical Abstract

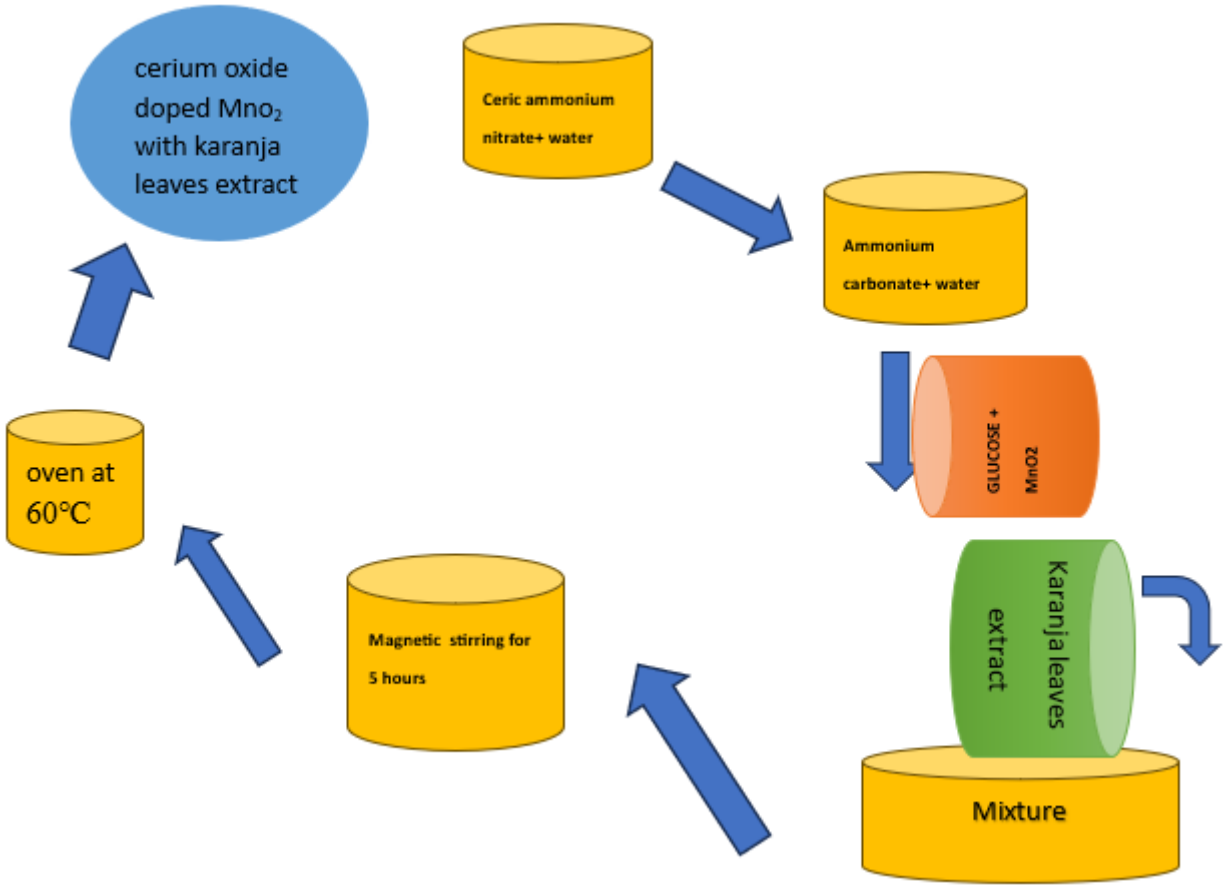

Figure 1. Graphical abstract of Synthesising CeO_2 doped with MnO_2 nanoparticles with karanja extract

2.2 Agarwell diffusion method

2.2.1 Anti-fungal

The anti-fungal agent present in the given sample was allowed to diffuse out into the medium and interact in a plate freshly seeded with the test organisms. The resulting zones of inhibition will be uniformly circular as there will be a confluent lawn of growth. The diameter of zone of inhibition can be measured in millimeters.

2.2.2 Materials required

Potato dextrose agar medium, Amphotericin B antimycotic solution, test samples, test tubes, beakers conical flask, spirit lamp, double distilled water and petri-plates.

2.2.3 Disc diffusion method

Potato dextrose agar medium

The potato dextrose agar medium was prepared by dissolving 20 gm of potato influsion, 2 gm of dextrose and 1.5 gm of agar in 100ml of distilled water. The dissolved medium was autoclaved at 15 lbs pressure at 121°C for 15 minutes. The autoclaved medium was mixed well and poured onto 100mm petri plates (25-30 ml/plate) while still molten.

Procedure

Petri plates containing 20ml potato dextrose agar medium was seeded with 72 hr culture of fungal strain *(*Aspergillus niger and Aspergillus fumigatus*)* different concentration of sample Extract (500, 250, 100

and 50 µg/ml) was added. The plates were then incubated at 28°C for 72 hours. The anti-fungal activity was assayed by measuring the diameter of the inhibition zone formed around the wells. Amphotericin B was used as a positive control. The values were calculated using Graph Pad Prism 6.0 software (USA).

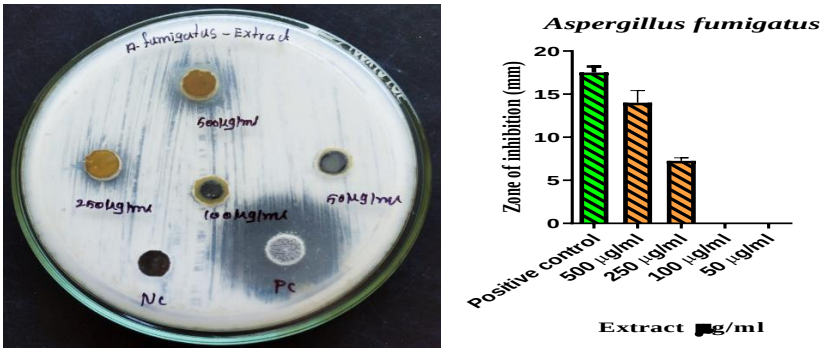

Figure 2. Effect of cerium oxide doped with MnO_2 + Extract against *Aspergillus fumigatus*

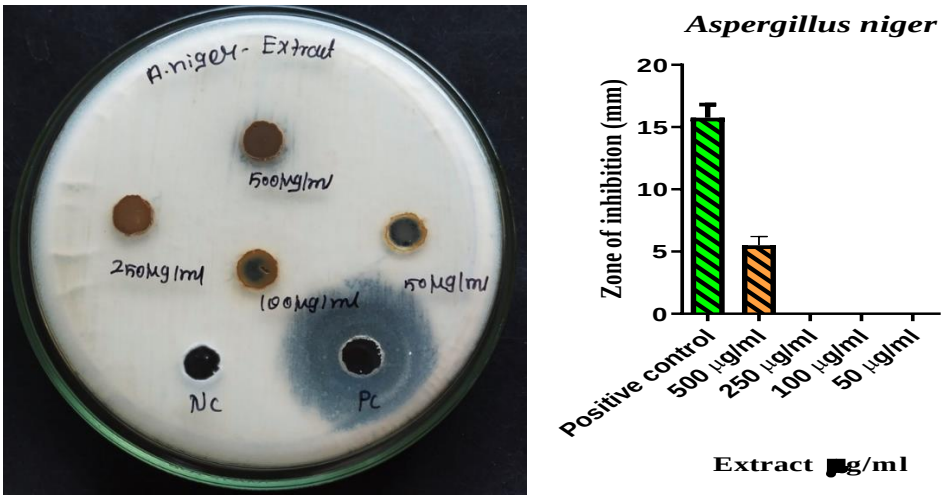

Figure 3. Effect of cerium oxide doped with MnO_2 +Extract against *Aspergillus niger.*

Table 1. SD± Means of zone of inhibition obtained by sample Extract against Aspergillus niger and Aspergillus fumigatus.

S.No	Name of the test organism	Name of the sample	Zone of inhibition (mm) SD ± Mean				
			500 µg/ml	250 µg/ml	100 µg/ml	50 µg/ml	PC
1.	*Aspergillus niger*	CeO_2 doped with MnO_2 + extract	5.5±0.70	0	0	0	15.75±1.06
2.	*Aspergillus fumigatus*		14±1.41	7.25±0.35	0	0	17.5±0.707

SD – Standard Deviation, *Significance - $p< 0.05$

Cerioum oxide doped with MnO_2 nanoparticles with karanja leaves extract exhibited antifungal activity with diferent concentrations (500 µg/ml, 250 µg/ml,100 µg/ml and 50 µg/ml)
as shown in the Table 1. The proposed mechanism of antifungal activity in various steps. Firstly, free radical ions released by CeO_2+MnO_2 NPs are tied with protein complex of fungi making an impact on the function of membrane and interact with living cells. Secondly NPs dissociate the cell structure. Then main cellular functions such as transportation are stopped progressively by the release of ions and consequent interactions. Further, the mitochondrial membrane zone was targeted by the free radicals produced by the synthesised nanoparticles during the interaction with external photons. Moreover, reactive oxygen species are released by the nanoparticles affect the central nucleic core structure of fungi and dismantle the whole structure [28]. Overall free radicals, ROS and metal ions destroys the fungal structure results in a complete cell inactiveness as shown in Figures 2-3.

3. Antimicrobial method

The antimicrobials present in the given sample were allowed to diffuse out into the medium and interact in a plate freshly seeded with the test organisms. The resulting zones of inhibition will be uniformly circular as there will be a confluent lawn of growth. The diameter of zone of inhibition can be measured in millimeters.

3.1 Materials required

(E.coli-443 and Staphylococcus aureus- 902*)* was purchased from MTCC, Chandihar, India. Nutrient Agar medium, Nutrient broth, Gentamicin antibiotic solution was purchased from Himedia, India. Test samples, petri-plates, test tubes, beakers conical flasks were from Borosil, India. Spirit lamp, double distilled water.

3.2 Agar-well diffusion method

3.3 Nutrient agar medium

The medium was prepared by dissolving 2.8 g of the commercially available Nutrient Agar Medium (HiMedia) in 100ml of distilled water. The dissolved medium was autoclaved at 15 lbs pressure at 121°C for 15 minutes. The autoclaved medium was mixed well and poured onto 100mm petriplates (25-30ml/plate) while still molten.

3.4 Nutrient broth

Nutrient broth was prepared by dissolving 2.8 g of commercially available nutrient medium (HiMedia) in 100ml distilled water and boiled to dissolve the medium completely. The medium was dispensed as desired and sterilized by autoclaving at 15 lbs pressure (121ºC) for 15 minutes. **3.5 Procedure**

Petri plates containing 20 ml nutrient agar medium were seeded with 24 hr culture of bacterial strains were adjusted to 0.5 OD value according to McFarland standard, (E.coli-443 and Staphylococcus aureus- 902) Wells were cut and concentration of sample Extract (500, 250, 100 and 50 µg/ml) was added
The plates were then incubated at 37°C for 24 hours. The antibacterial activity was assayed by measuring the diameter of the inhibition zone formed around the wells. Gentamicin antibiotic was used as a positive control. The values were calculated using Graph Pad Prism 6.0 software (USA).

3.5 Results

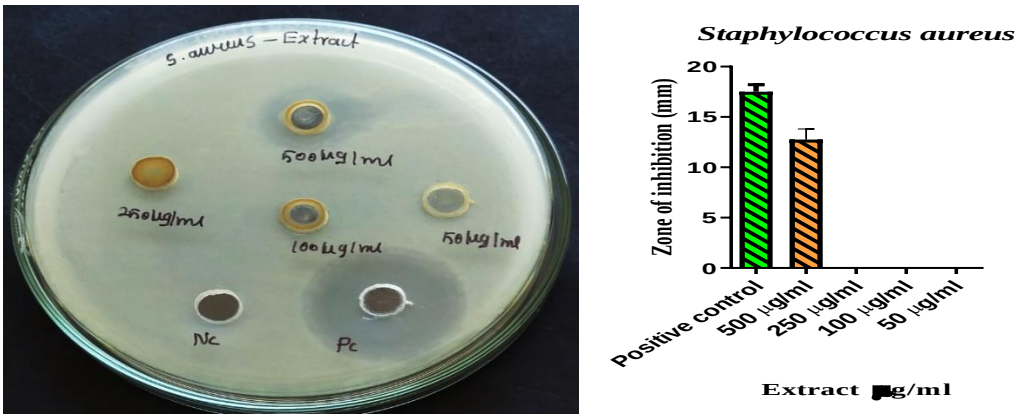

Figure 4. Effect of sample Extract against Staphylococcus aureus

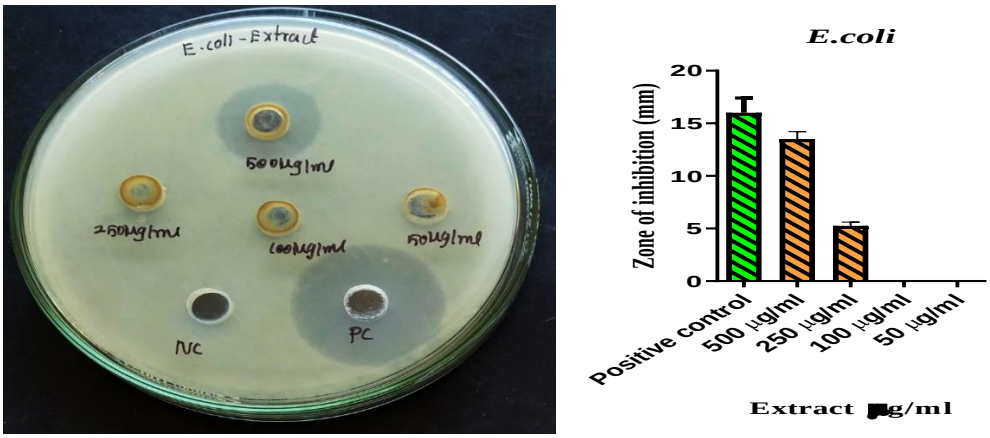

Figure 5. Effect of sample Extract against E.coli.

Table 2. Means ± SD of zone of inhibition obtained by sample Extract against E.coli and Staphylococcus aureus.

S. No	Name of the test organism	Name of the test sample	Zone of inhibition (mm) Mean±SD				
			500 µg/ml	250 µg/ml	100 µg/ml	50 µg/ml	PC
1.	*E.coli*	Extract	13.5±0.70	5.25±0.35	0	0	16±1.41
2.	*Staphylococcus aureus*		12.75±1.06	0	0	0	17.5±0.7

SD – Standard Deviation, *Significance - $p< 0.05$

The antibacterial efficiency of Cerium oxide doped with MnO_2 nanoparticles with karanja leaves extract with diferent concentrations (500 µg/ml, 250 µg/ml,100 µg/ml and 50 µg/ml) as shown in the Table 2 based upon the following factors (a) percentage of reactive oxygen species (ROS), (b) percentage of cations delivered and (c) geometrical nature of particles and its volume. From the theory of electromagnetic waves, if a light radiation with energy that matches with the band gap of Cerium oxide doped with MnO_2 interacts, electronic excitation from the lower energy level to higher energy levels say valence band to conduction band takes place leaving a hole in the VB, then the following reaction takes

place i)The electrons at higher energy levels (CB) as well as holes formed in the lower energy level (VB) induce the emanation of the entities such as hydrogen peroxide (i) hydroxyl radical ions (HRI) (ii) reactive oxygen species (ROS), super oxide anion $(O^{\cdot})^{-}$ (SOA) in the environment: The ROS damage the cell membrane leads to dissociation of DNA, plasmid, ribosome, cytoplasm, cytoplasmic membrane, cell wall, capsule and nucleoid takes place which inactivate bacteria. ROS are produced when the holes interact with the $O_2^{\cdot-}$ [23]. The reaction as follows

$$\mathbf{CeO_2 : MnO_2 + h \rightarrow CeO_2 : MnO_2 + h^+ + e^-}$$

$$\mathbf{O_2 + e^- \rightarrow O_2^{\cdot-}}$$

$$\mathbf{O_2^{\cdot-} + H^+ \rightarrow HO^{\cdot}}$$

$$\mathbf{H^+ + HO^{\cdot}\,^2 + e^- \rightarrow H_2O_2}$$

$$\mathbf{H_2O_2 + O_2^{\cdot-} \rightarrow OH^{\cdot} + O_2 + OH}$$

i)The participation of ions and oxides takes place according to Haber–Weiss reaction theory where hydroxyl and hydroxide ions are produced due to the reaction of H_2O_2 and superoxide ion.ii) When compare the reaction of H_2O_2 with that of ROS, the former is less toxic in nature and makes abnormal dissociation with bacteria.iii) It also give $OH^{\bullet}$ radicals when H_2O_2 reacts with SOA($O_2^{\cdot-}$) .CeO_2 : MnO_2 NPs are smaller than bacterial pores, they can penetrate the cell membrane and cause cell death of the bacterial strain [33]. The bar diagram shows ZOI in Figure 4-5. and Table 2. From the bar diagrams zone of inhibition results, it is found that CeO_2 : MnO_2 NPs extract exhibits the highest antibacterial efficiency when compared with the other samples, also shows a remarkable ZOI even at lower concentrations. The above three factors are responsible for effective antibacterial activity [34–36].

4. Photo catalytic degradation studies using UV- Visible spectroscopy

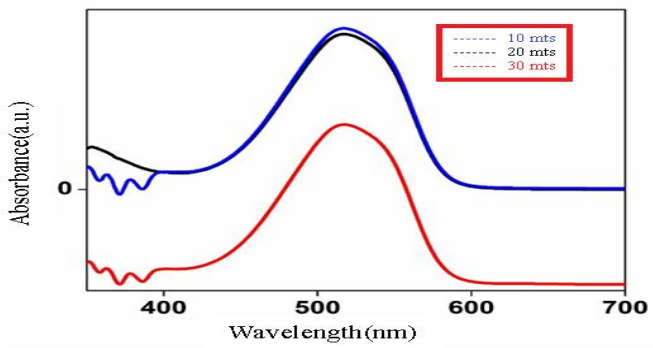

Figure 6. Photocatalytic degradation curve

The visible light source is a 350 W xenon lamp with JASCO-V730 ultraviolet cutoff filter and visible light reflection filter (through 420–780 nm visible light).The whole data of photocatalytic activity was observed in a photoreactor equipped with lamp intensity of 6.0 mW cm^{-2} placed at a distance 25 cm at 25°C .The synthesised Nps photocatalytic activity was tested by using methylred as the pollutant dye under visible and ultraviolet (UV) radiation. In this photo catalytic process, 2.5 mg of a sample was taken and added 10 mL of purely dissolved in water medium of methylred. The spectroscopic analysis of the reaction mixture of doping Mn in CeO_2 and methylred dye solution are exposed to visible and UV radiation in photo reactor revealed that a gradual decrease in the absorbance intensity with time. The concentration of methylred dye decreases in the solution is due to photocatalytic degradation. The photocatalytic efficiency of pure CeO_2 NPs was found to be 39.4 and 43.2 % under visible and UV irradiation respectively. The highest

efficiency was observed for 2 mol % Mn-doped CeO_2 nanoparticles. It was found to be 61.45 % for photocatalytic degradation under visible and UV irradiation.

It is important to note that there is decrease in band gap due to doping of Mn in CeO_2 creates oxygen vacancies and converts Ce(IV) ions to Ce(III) ions.Ce(III) ions are responsible for creating localized energy states which are closer to conduction band and decrease the band gap. The mechanism of photo-catalytic degradation lies in the fact that upon excitation with photons of sufficient energy, the electron from valence band of photocatalyst jump to the conduction band, leaving behind a positive hole in the valence band. These charge carriers migrate to the surface of the catalyst, interact with the adsorbed species and initiate redox reactions leading to photocatalysis. The surface interaction of charge carriers with the adsorbed species can take place in a number of ways.

Positive holes can interact with water forming strong oxidizing hydroxyl free radicals(·OH),which in turn can oxidize adsorbed dye molecules. On the other hand, electrons in the conduction band can combine with oxygen molecules present at the surface of catalyst reducing it to superoxide ion $(_{O_2})^-$. This species may undergo secondary reactions to give hydroperoxylradical(·OOH) and H_2O_2. These are initiating oxidative paths for dye degradation [37]. In this case, doping of Mn ions to CeO_2 Nps results decrease in band gap. It also facilitates photogeneration of charge carriers (electron and hole) by exciting the electron from valence band to conduction band even by visible radiation in doped nanoparticles [38]. These charge carriers reactions to give oxidizing species. This photocatalytic degradation takes place at the surface or within a few monolayers around it [39].

5. X-ray diffraction

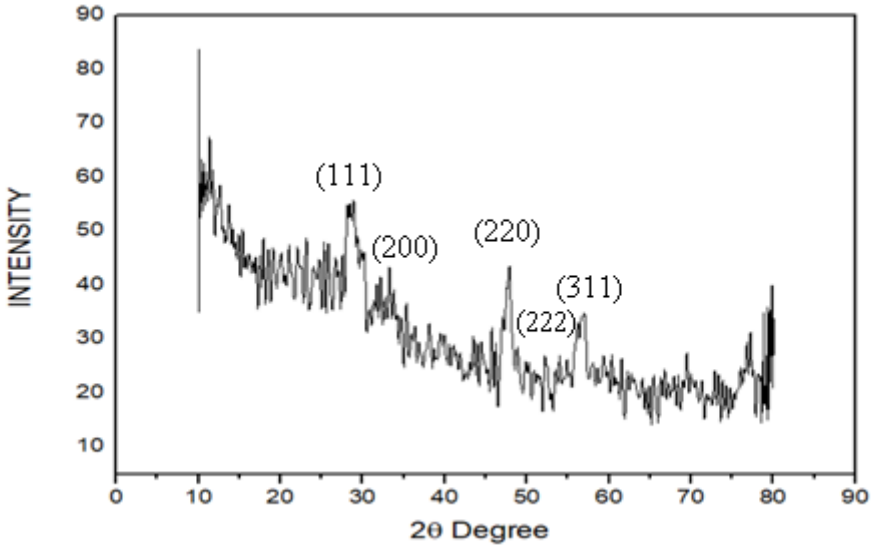

Figure 7. XRD analysis of CeO_2 doped with MnO_2 with karanja extract

An intense method of X-ray powder diffraction (XRD) was utilized to discover the crystalline phase which is available in materials. It is also useful to measure the structural properties of those phases. X-ray powder diffraction patterns of the pure and the Mn-doped CeO_2 nanoparticles are shown in Figure 7. The excellent peaks (111), (200), (220),(222), (311) were obtained. The investigation of peak broadening was required as a result of the tiny grain size of CeO_2 nanoparticles [20]. As the Mn content inCeO_2 nanoparticles increased, the intensity of XRD peaks decreased which demonstrated the degradation of crystallinity. The average grain size of Mn-doped CeO2 nanoparticles has been determined using the Scherrer formula:

$$D = 0.9\lambda/\beta \cos\theta \quad (1)$$

where λ is the X-ray wavelength, θ is the Bragg diffraction angle and β is the full width at half maximum (FWHM) of the XRD peak appearing at the diffraction angle θ. The average grain sizes of the pure and the Mn-doped CeO_2 nano-particles were observed to be 12 and 14 nm, respectively.

The grain sizes were evaluated from the Scherrer's relation. It showed that increases in the dopant concentration of Mn increased the average grain size. The lattice parameter decreased with increasing the dopant concentration of Mn. It was understood that Mn doping in CeO_2 produced crystal defects around the dopants and the charge imbalance arising from this imperfection changed the stoichiometry of the materials. XRD analysis proves that crystalline structure of CeO_2 Fluorite and those peaks are seen at 28° and 47° due to the diffraction planes of (1 1 1) and (2 2 0) [JCPDS.No.34-0394] which are raised by the cerium concentration.The diffraction peaks at 32.8°, 49°, 55° are attributed in good agreement with JCPDS. No.44-0141. It has α-MnO_2 with tetragonal structure [40].

6. Scanning electron microscopy

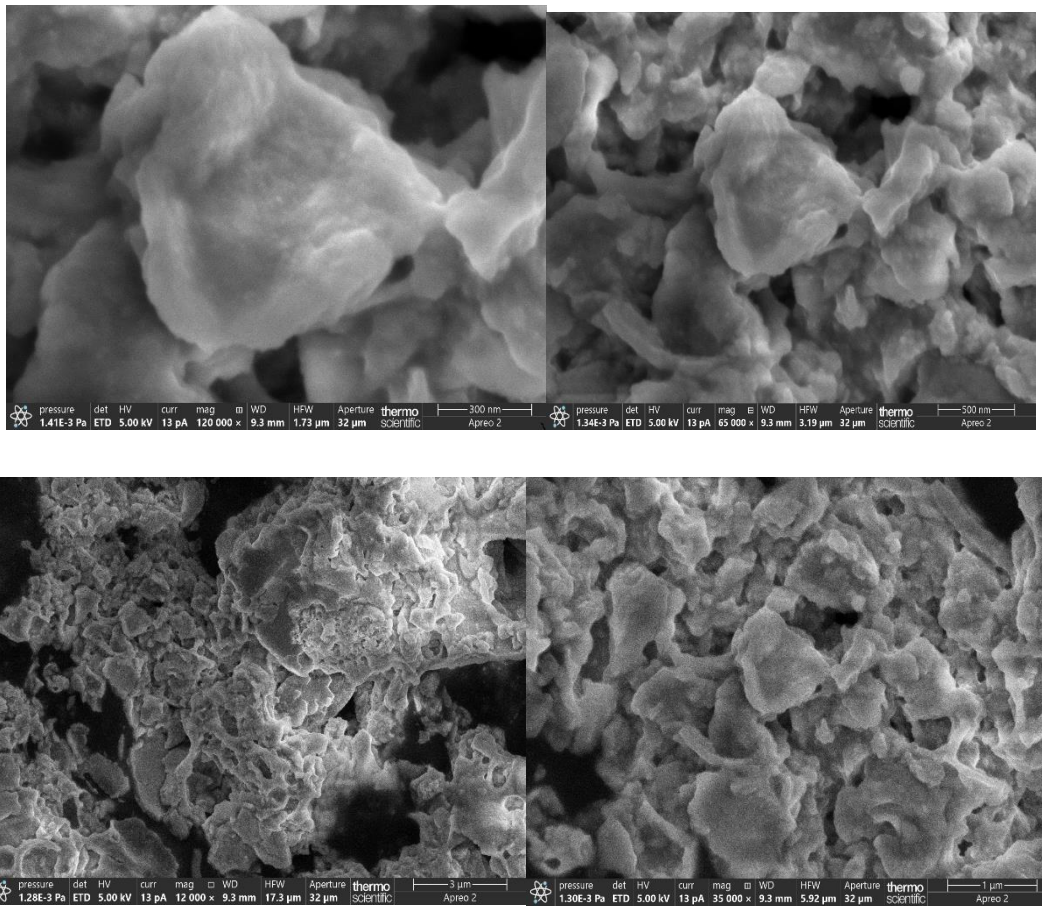

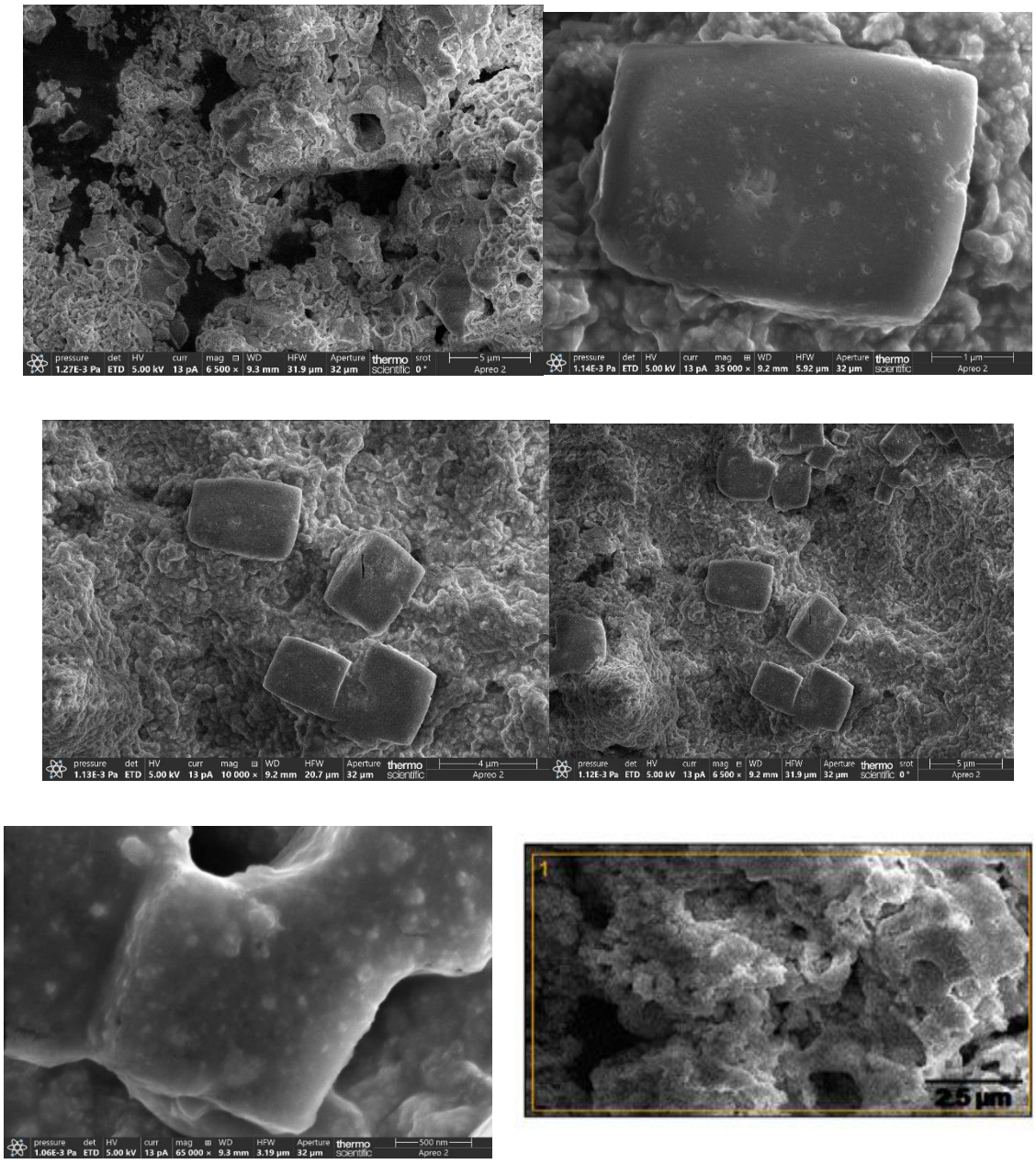

Figure 8. SEM images of Cerium oxide doped MnO_2 with karanja extract

Scanning electron microscopy (SEM) is one of the most widely used techniques for the characterization morphology of the particles. The SEM pictures of the pure and the Mn-doped CeO_2 nanoparticles are shown in Figure 8. It is clearly observed that the particles that are highly aggregated are of permeable nature. There are small agglomerated particles and this may be because of the lower calcination temperature. This affirms the decrease in crystalline size essentially by adding Mn particles to CeO_2 host .Figure 8 depict the observed SEM images of Manganese Dioxide, doped with CeO_2 . MnO_2 has a systematic morphology with agglomeration. Both the Ceriumoxide and doped MnO_2 have spherical like structure with massive agglomeration. Particles are distributed nonuniformly. This could be due to the loading of MnO_2 into cerium oxide NPs. The main reason for the occurrence of agglomeration is interfacial surface tension formed at the surface of the doped samples[41]..

7. EDAX Analysis

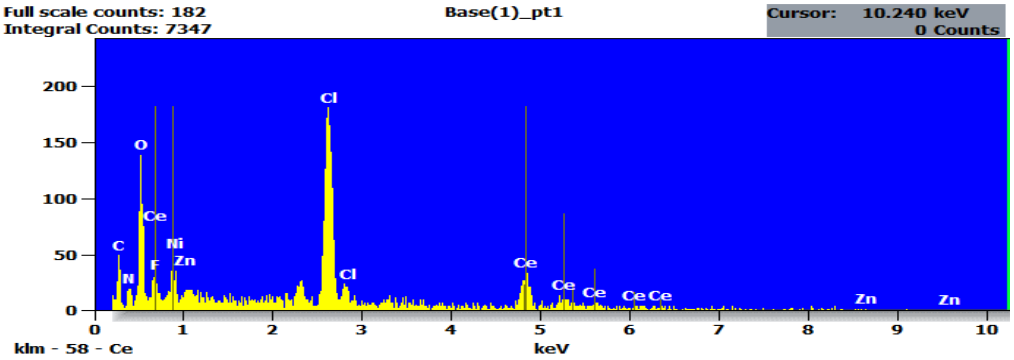

Figure 9. EDAX Analysis of Cerium oxide doped MnO_2 with karanja extract

The Composition of the elements for the synthesized samples has been inspected by energy dispersive X-ray spectroscopy shown by Figure 9. The presence of composition elements like Carbon (C), Nitrogen(N), Oxygen (O) Fluorine(F), Chlorine(Cl) ,Nickel(Ni), Zinc(Zn),Manganese(Mn) and Cerium(Ce) were confirmed by EDAX analysis.The weight composition obtained from EDS analysis of the normalized spectrum was Ce,Mn and oxygen.EDS also revealed that the formation of N, Zn which shows better antibacterial activity.

Table 3. EDAX Analysis of elements

Element	Net counts	Weight %	Atom%
C	232	5.47	15.14
N	108	4.59	10.88
O	617	14.35	29.80
F	114	2.37	4.14
Cl	1956	30.66	28.73
Ni	131	2.51	1.42
Zn	57	142	0.72
Ce	424	38.63	9.17
Total		100.0	100.0

8. Infra-red spectroscopy

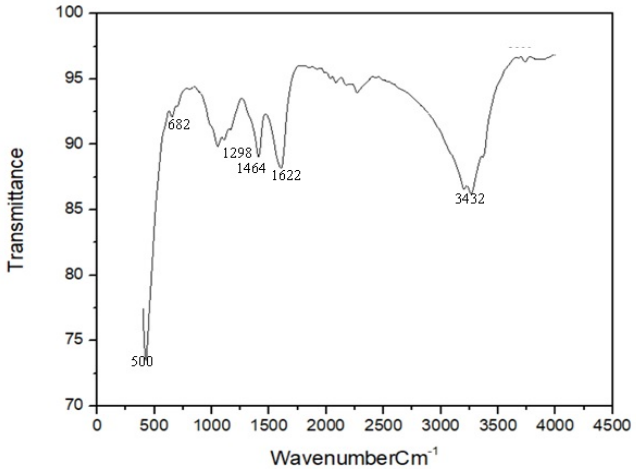

Figure 9. FT IR spectrum of MnO_2 doped CeO_2 with karanja extract

FT IR spectrum of MnO_2doped ceriumoxide with karanja is shown in figure 9. Three strong absorption bands at 3432,1622 and 1464 cm^{-1}belongs to symmetric stretching of O-H bending methods of inside bonded water molecules and bending vibrations of C-H stretching.The bending mode of Ce-O-C was seen below 682cm^{-1} belongs to formation of CeO_2 without impurities, 500 cm^{-1}belongs to Ce-O stretching vibration 1298cm^{-1}belomgs to carbonate species.

9. Conclusion

It is concluded that Mn doped cerium oxide Nps with karanja leaves extract have better antimicrobial and antifungal activity. It has good photo degradation activity in methyl red medium.All the activities are proved by characterisation techniques of UV, XRD,SEM,EDAX FT-I , Agarwell-diffusion method and Disc- diffusion method.

References

1. Wang,Y,; Wang,Z,; Muhammad,S,; and He,J,; *Cryst EngComm*. **2012**,14,5065.https://doi.org/10.1039/c2ce25517k.
2. Higashimoto, S,; Tanaka,Y,; Ishikawa,R,; Hasegawa, S,; Azuma, M,; Ohue,H,; and Sakata,Y,; *Catal. Sci. Technol*. **2013,** 3,400. https://doi.org/10.1039/C2CY20607B.
3. Trovarelli,A,; De Leitenburg, C,; Boaro,M,;and Dolcetti, G,;*Catal. Today*.**1999,**50,353. https://doi.org/10.1016/S0920-5861(98)00515-X.
4. Li,R,X,; Yabe,S,; Yamashita,M,; Momose,S,; Yoshida,S,; Yin,S,; and Sato,T,; *Solid State Ion*.**2002**,151, 235. https://doi.org/10.1016/S0167-2738(02)00715-4.
5. Masui,T,; Hirai,H,; Hamada,R,; Imanaka,N,; Adachi,G,; Sakata,T,; and Mori,H,; *J. Mater. Chem*. **2003**,13,622. https://doi.org/10.1039/b208109a.
6. Liu,I,; Hon,M.H.; and Teoh,L.G,; *J. Electron. Mater*.**2013**, 42, 2536. https://doi.org/10.1007/s11664-013-2617-9.
7. Saranya, J,; Ranjith,K.S,; Saravanan,P,; Mangalaraj,D,; and Rajendra Kumar,R.T,; *Mater. Sci. Semicond. Process*. **2014**,26,218. https://doi.org/10.1016/j.mssp.2014.03.054.
8. Herrling,T,; Seifert ,M,;and Jung,K,; SOFW J,;2013,12,139. Pouretedal,H,R,; and Kadkhodaie,A,; *Chin. J. Catal*.**2010**,31,1328. https://doi.org/10.1016/S1872-2067(10)60121-0.
9. Mohamed,R,M,; and Aazam,E,S,; *Int. J. Photoenergy*, Article ID 137328 **2011**.https://doi.org/10.1155/2011/137328.
10. Sifontes,A,B,; Rosales,M,; Méndez,F,J,; Oviedo,O,; and Zoltan,T,J,;**2013,**1. Nanomater., 2013, 1 (2013); https://doi.org/10.1155/2013/265797.
11. Akbari-Fakhrabadi, A,; Saravanan,R,; Jamshidijam, M,; Mangalaraja,R,V,; and Gracia,M,A,; *J. Saudi Chem. Soc*.**2015,**19,505. https://doi.org/10.1016/j.jscs.2015.06.003.
12. Li,W,; Liang,R,; Hu,A,; Huang,Z,; and Zhou,A,N,; *RSC Adv*.**2014**,4,36959. https://doi.org/10.1039/C4RA04768K.
13. Liyanage,A,D,; Perera,S,D,; Tan,K,; Chabal,Y,; and Balkus,K,J,; *Jr. ACS.* **2014**,4,457. https://doi.org/10.1021/cs400889y.
14. Channei,D,; Inceesungvorn,B,; Wetchakun,N,; Ukritnukun,S,; Na ttestad,A,; *J. Chen and S. Phanichphant, Sci. Rep*.**2014**, 4, 5757. https://doi.org/10.1038/srep05757.
15. Primo,A,; Marino,T,; Corma,A,; Molinari,R,; and García, H,;*J. Am. Chem*.**2011**,133,6930 https://doi.org/10.1021/ja2011498.

16. Liang,H,; Raitano,J,M,; He,G,; Akey,A,J,; Herman,I,P,; Zhang,L,; and Chan,S,W,; *J. Mater. Sci.***2012**, 47, 299. https://doi.org/10.1007/s10853-011-5798-8.
17. Tan,J,; Zhang,W,; Lv,Y,H,; and Xia,A,L,; *Mater. Res.***2013**, 16, 689. https://doi.org/10.1590/S1516-14392013005000040.
18. Yue,L.; and Zhang,X,M,; *J. Alloys Compd.***2009**, 475, 702. https://doi.org/10.1016/j.jallcom.2008.07.096.
19. Montini,T,; Melchionna,M,; Monai,M,; and Fornasiero,P,; *Chem. Rev*.**2017**,116,5987. https://doi.org/10.1021/acs.chemrev.5b00603.
20. Herrera, F,; Kiwi, J,; Lopez,A,; and Nadtochenko,V,; *Environ. Sci. Technol*.**1999**,33,3145. https://doi.org/10.1021/es980995
21. Dua,T,K,; Giri,S,; Nandi,G,; Sahu,R,; Shaw,T,K,; Paul,P,; Green synthesis of silver nanoparticles using Eupatorium adenophorum leaf extract characterizations, antioxidant, antibacterial and photocatalytic activities. *Chem Pap*,**2023**, 77,2947–2956.
22. Suresh,S,; Ilakiya,R,; Kalaiyan,G,; Thambidurai,S,; Kannan,P,; Prabu,K,M,; Suresh,N,; Jothilakshmi,R,; Karthick Kumar,S,; Kandasamy,M,; Green Synthesis of copper oxide nanostructures using Cynodon dactylon and Cyperus rotundus grass extracts for antibacterial applications. *Ceram Int*. **2020**,46(8),12525–12537.
23. Theophil Anand,G,; John Sundaram,S,; Kanimozhi,K,; Nithiyavathi,R,; Kaviyarasu,K,; Microwave assisted green synthesis of CuO nanoparticles for environmental applications. *Mater Today Proc*,**2021**,36,427–434.
24. Birhanu,R,; Afrasa,M,A,; Hone,F,G,; recent progress of advanced metal-oxide nanocomposites for efective and low-cost antimicrobial activates, a review. *J Nanomater*. **2023**,1–25.
25. Sithi Asma,B,; Palanimurugan,A,; Dhanalakshmi,A,; Thangadura,S.; Synthesis and characterization of favored transition metal ions using Datura metel seed extracts and its better antimicrobial activity. *Materials today proceedings*. **2022**,68,515–522.
26. Emima Jeronsia,J,; Allwin Joseph,L,; Annie Vinosha,P,; Jerline Mary,A,; Jerome Das,S,; Camellia sinensis leaf extract mediated synthesis of copper oxide nanostructures for potential biomedical applications. *Mater Today Proc*.**2019**, 8,214–222.
27. Weldegebrieal,G,K,; Photocatalytic and antibacterial activity of CuO nanoparticles biosynthesized using Verbascum thapsus leaves extract. *Optik*. **2020**,204,1–11.
28. Melda,A,; Azade,A,; Fatih,E,; Corina Marilena Cristache, Ibrahim Isildak, Fresenius Green synthesis of copper oxide nanoparticles using Ocimum basilicum extract and their antibacterial activity. *Fresenius Environ Bull*.**2017** 26,7832–7837.
29. Gnanadesigan,M,; Anand, M,; Ravikumar,S,; Maruthupandy,M,; Syed Ali, M,; Vijayakumar, V,; Kumaraguru,A,K,; Antibacterial potential of biosynthesised silver nanoparticles using Avicennia marina mangrove plant. Appl Nanosci **2012**,2-1,143–147.
30. Sivaraj,R,; Rahman,P,K,S,M,; Rajiv,P,; Narendhran,S,;Venckatesh,R,; Biosynthesis and characterization of Acalypha indica mediated copper oxide nanoparticles and evaluationof its antimicrobial and anticancer activity. *Spectrochim Acta Part A Mol Biomol Spectrosc*. **2014**,129,255–258.
31. Acharyulu,N,P,S,; Dubey,R,S,; Swaminadham,V,; Kalyani Pratap Kollu,R,L,; Pammi,S,V,N,; Green synthesis of CuO nanoparticles using Phyllanthus amarus leaf extract and their antibacterial activity against multidrug resistance bacteria. *Int J Eng Res Technol*.**2014**,3,639–641.

32. Choudhary,B,P,; Rai,S,; Singh,N,B,; Green synthesis of pure and silver doped copper oxide nanoparticles using Moringa oleifera leaf extract. *Emerg Mater Res*.**2017**, 6,285–295.
33. Amiri,M,R,; Alavi,M,; Taran,M,; Kahriz,D,; Antibacterial, antifungal, antiviral, and photocatalytic activities of TiO2 nanoparticles, nanocomposites, and bio-nanocomposites: recent advances and challenges. *J Public Health Res* **2022**,7,1–6
34. Sankar,R,; Manikandan,P,; Malarvizhi,V,; Fathima,T,; Shivashangari,K,S,; Ravikumar,V,; Green synthesis of colloidal copper oxide nanoparticles using Carica papaya and its application in photocatalytic dye degradation. *Mol Biomol Spectrosc Spectrochim Acta Part A*. **2014**,121,746–750.
35. Sheikh,M,C,; Hasan,M,M,; Hasan,M,N,; Salman,M,S,; Kubra,K,T,; Awual, M,E,; Waliullah,R,M,; Rasee A,I,; Rehan,A,I,; Hossain,M,S,; Marwani,H,M,; Islam,A,; Khaleque,M.S,;Awual,M,R,; Toxic Chemistry Africa cadmium (II) monitoring and removal from aqueous solution using ligand-based facial composite adsorbent. *J Mol Liq*.**2023**, 389,122854.
36. Tachikawa,T, Fujitsuka,M,; and Majima,T,; *J. Phys. Chem. C*,**2007**, 111, 5259. https://doi.org/10.1021/jp0
37. Sun,Y,; Qu,B,; Liu,Q,; Gao,S,; Yan,Z,; Yan,W,; Pan,B,; Wei,S,; and Xie,Y,; *Nanoscale*.**2012**, 4, 3761. https://doi.org/10.1039/c2nr30371j.
38. Chatti,M,; Adusumalli,V,N,K,B, S,; Ganguli and Mahalingam,V,; *Dalton Trans*.**2016**, 45, 12384. https://doi.org/10.1039/C6DT02548J.
39. Tscho”pe,A,; Sommer,E,; Birringer,R,;*Solid State Ionics*.**2001**,138,255-265.
40. Choi,J,; Amaranath Reddy,D,; Jahurul Islam,; Ma,R,; Kim,T,K,; *J..alloy.Compd*.**2016,**688,527-e536.